

Exploration of Spin-Dependent Thermoelectricity in the Chiral Double-Stranded DNA Molecule Coupled to Ferromagnetic Leads

Lei-Lei Nian,¹ Long Bai,^{1,*} Wenting Yu,¹ Jun Tang,¹ Huichao Li,¹ Rong Zhang,¹ Rui-Qiang Wang,² Xue-Feng Wang,^{3,†} and M. Wierzbicki⁴

¹*School of Physical Science and Technology, China University of Mining and Technology, Xuzhou 221116, China*

²*Guangdong Provincial Key Laboratory of Quantum Engineering and Quantum Materials, School of Physics and Telecommunication Engineering, South China Normal University, Guangzhou 510006, China*

³*School of Physical Science and Technology, Soochow University, Suzhou 215006, China*

⁴*Faculty of Physics, Warsaw University of Technology, ul. Koszykowa 75, 00-662 Warsaw, Poland*



(Received 6 May 2018; revised manuscript received 18 June 2019; published 13 August 2019)

Double-stranded DNA (dsDNA) molecules possess a unique chirality, where chirality-induced spin selectivity offers the promise of organic-molecule-based spintronic devices, and they have become an interesting field of their own. When coupled to ferromagnetic leads, such systems, when driven by a temperature gradient, are expected to manifest new thermoelectric behaviors. Herein, we investigate the spin-related thermoelectricity of a chiral dsDNA molecular junction in terms of linear response theory and the nonequilibrium Green's function formalism. Not only is a strong violation of the Wiedemann-Franz law found in the charge-Seebeck transport regime, but the spin figure of merit is also larger than unity. More interestingly, a finite spin-Seebeck coefficient with a charge thermopower of zero can be obtained, which may serve as a pure spin-current generator. The detailed dependence of the basic thermoelectric quantities on the system parameters is elaborated on, and the underlying physics is presented. Our results have substantial implications for the construction of spin caloritronic devices based on dsDNA or other chiral molecules.

DOI: 10.1103/PhysRevApplied.12.024025

I. INTRODUCTION

In recent years, substantial improvements have been made in understanding the physical mechanisms of electronic transport through DNA molecules since charge migration in DNA was first suggested by Eley and Spivey [1]. As the genetic code of all living species, DNA has a special double-helix structure which is made up of four nucleotides. Four nucleobases [i.e., guanine (G), cytosine (C), adenine (A), and thymine (T)] corresponding to four nucleotides form two base pairs (G-C, A-T) via hydrogen bonds, and the π - π overlap of the stacked base pairs in double-stranded DNA (dsDNA) chains can be regarded as the main conducting pathway for charge transfer. Indeed, DNA molecules can exhibit diverse conduction characteristics. The experimental work of Yoo *et al.* indicated that double-stranded poly(dA)-poly(dT) and poly(dG)-poly(dC) chains behave as *n*-type and *p*-type semiconductors, respectively [2]. Storm *et al.* reported that DNA molecules have an insulating behavior [3]. Some experimental results have demonstrated that DNA can be

a conductor [4–7], even the proximity-induced superconductivity can be observed [8]. From the point of view of theoretical investigations, a series of methods have been developed to study the electronic transport behavior of DNA molecules, such as the transfer matrix method [9,10], the nonequilibrium Green's function technique [11–13], *ab initio* calculations [14], and so forth. It is instructive to note that, to date, DNA has played a significant role in the design of molecular electronic devices due to its unique versatile and programmable structure [15–21]. What is more, recent investigations of spin-dependent transport through DNA molecules have shown that DNA has tremendous potential for engineering novel spin-based electronic devices [22–29].

It is well known that the thermoelectric efficiency, characterized by the figure of merit $ZT = GS^2T/\kappa$ for conventional materials, where G is the electrical conductance, S represents the thermopower (Seebeck coefficient), T is the temperature, and κ denotes the thermal conductance (which contains both electronic and phononic contributions), is relatively low due to the restrictions imposed by the Wiedemann-Franz (WF) law. However, nanoscale materials can overcome the WF law and exhibit better thermoelectric performance than that of conventional

*bailong2200@163.com

†wxsf@suda.edu.cn

bulk materials. Recent achievements in observation of the thermoelectric (i.e., Seebeck) effect in nanoscale systems (e.g., quantum dots [30–36], nanowires [37–40], graphene [41–43], and topological insulators [44,45]) have also invigorated intensive interest in molecular junctions [46–49], including DNA [50–55]. By means of the Mott formula and an effective model Hamiltonian for DNA, Maciá theoretically studied the Seebeck effect in DNA coupled to metallic leads [50–52], and found that a junction with a DNA-based molecule exhibited significant thermoelectric performance, which suggested that DNA could become a novel thermoelectric material from the application point of view. On the basis of a tight-binding (TB) ladder model, recent work has demonstrated that quantum interferences induced by intrastrand and interstrand coupling contribute remarkably to the thermoelectric efficiency of the DNA molecule [53]. Although there exist some results on the thermoelectricity of DNA molecules, these investigations usually assume that dsDNA is a linear lattice chain based on an effective TB model. Note that dsDNA, as an important biomolecule, has an obvious spatial structure with chirality breaking the parity symmetry. Moreover, theoretical calculations and experimental measurements have unequivocally demonstrated that the chirality-induced spin selectivity (CISS) effect in three-dimensional dsDNA molecules significantly influences the electronic transport process [25–27,56–61]. As a consequence, the chiral nature of dsDNA molecules plays an important role in any precise understanding of the spin-related thermoelectric properties of the dsDNA molecule. The aim of this paper is to shed light on the spin-dependent thermoelectricity of the chiral dsDNA system, and provide deep insights into the thermoelectric transport of dsDNA. By tuning the parameters of a chiral dsDNA molecular junction, we demonstrate in our results that the thermoelectric features of chiral dsDNA open up the possibility of applications of thermoelectric devices based on chiral organic molecules.

The rest of this paper is organized as follows. We begin by presenting details of the chiral dsDNA molecular junction under investigation, and present the approach to studying the thermoelectric performance of the chiral dsDNA system in Sec. II. In Sec. III we analyze our numerical results, and we summarize our conclusions in Sec. IV.

II. PHYSICAL MODEL AND FORMALISM

A. Physical model

We consider a chiral dsDNA molecule bridging two ferromagnetic (FM) leads as depicted schematically in Fig. 1. The full system can be described by the following Hamiltonian:

$$H = H_{\text{leads}} + H_{\text{DNA}} + H_{\text{so}} + H_{\text{tun}}. \quad (1)$$

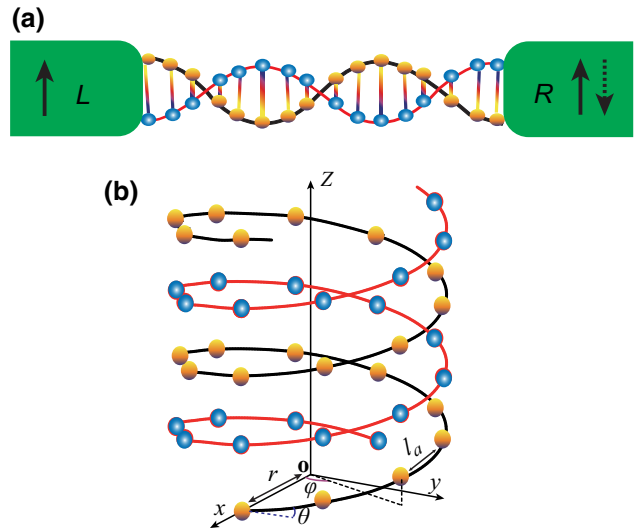


FIG. 1. (a) Geometry of the dsDNA connected to two FM leads used in this work. (b) Schematic representation of right-handed dsDNA with helix angle θ , radius r , arc length l_a , and cylindrical coordinate φ . The stacking distance Δh between two nearest-neighbor sites is $l_a \sin \theta$.

Here, H_{leads} models the Hamiltonian of the two FM leads and is given by

$$H_{\text{leads}} = \sum_{k,\sigma,v=L,R} \varepsilon_{kv\sigma} a_{kv\sigma}^\dagger a_{kv\sigma}, \quad (2)$$

where $a_{kv\sigma}^\dagger$ ($a_{kv\sigma}$) denotes the creation (annihilation) operator of an electron with spin σ ($=\uparrow, \downarrow$), momentum k , and energy $\varepsilon_{kv\sigma}$ in the left ($v = L$) and right ($v = R$) leads. The second term, H_{DNA} , in Eq. (1) describes the dsDNA molecule:

$$\begin{aligned} H_{\text{DNA}} = & \sum_{m=1}^2 \sum_{\sigma} \left\{ \sum_{n=1}^N \varepsilon_{mn} d_{mn\sigma}^\dagger d_{mn\sigma} \right. \\ & + \sum_{n=1}^{N-1} (t_{mn} d_{mn\sigma}^\dagger d_{mn+1\sigma} + \text{H.c.}) \Big\} \\ & + \sum_{n=1}^N (\lambda_n d_{1n\sigma}^\dagger d_{2n\sigma} + \text{H.c.}). \end{aligned} \quad (3)$$

Here, $m (= 1, 2)$ is the chain label, N denotes the number of base pairs, $d_{mn\sigma}^\dagger$ ($d_{mn\sigma}$) is the creation (annihilation) operator at the n th site of the m th chain of the dsDNA, and ε_{mn} is the on-site energy. t_{mn} and λ_n are the intrachain and interchain coupling parameters, respectively.

H_{so} in Eq. (1) represents the spin-orbit coupling (SOC) Hamiltonian within the chain, which comes from the double-helix shape of the electrostatic potential of the

dsDNA; H_{so} is given by Refs. [25–27]:

$$H_{\text{so}} = it_{\text{so}} \sum_{m,n} \sum_{\sigma,\sigma'} \left[d_{mn\sigma}^\dagger \left(\sigma_{n,\sigma\sigma'}^{(m)} + \sigma_{n+1,\sigma\sigma'}^{(m)} \right) d_{mn+1\sigma'} + \text{H.c.} \right], \quad (4)$$

where $\sigma_{n+1,\sigma\sigma'}^{(m)} = \sigma_{z,\sigma\sigma'} \cos \theta - (-1)^m [\sigma_{x,\sigma\sigma'} \sin(n \Delta\varphi) - \sigma_{y,\sigma\sigma'} \cos(n \Delta\varphi)] \sin \theta$, with the Pauli matrices $(\sigma_x, \sigma_y, \sigma_z)$, $\Delta\varphi$ as the twist angle between successive base pairs, θ as the helix angle, and t_{so} as the SOC strength. The last term, H_{tun} , in Eq. (1) describes the tunnel coupling between the dsDNA molecule and the two FM leads, and it can be given by

$$H_{\text{tun}} = \sum_{k,\sigma,v=L,R} \left[t_v a_{kv\sigma}^\dagger (d_{1n_v\sigma} + d_{2n_v\sigma}) + \text{H.c.} \right], \quad (5)$$

where, for simplicity, the hopping-matrix elements t_v between the leads and the dsDNA are assumed to be independent of both spin and momentum, with $n_L = 1$ and $n_R = N$. The two helical chains are coupled to the left lead at sites (1, 1) and (2, 1) and to the right lead at (1, N) and (2, N). We choose the following representation: $\Psi^\dagger = (d_{11\uparrow}^\dagger, d_{21\uparrow}^\dagger, d_{12\uparrow}^\dagger, d_{22\uparrow}^\dagger, \dots, d_{1N\uparrow}^\dagger, d_{2N\uparrow}^\dagger; d_{11\downarrow}^\dagger, d_{21\downarrow}^\dagger, d_{12\downarrow}^\dagger, d_{22\downarrow}^\dagger, \dots, d_{1N\downarrow}^\dagger, d_{2N\downarrow}^\dagger)$; thus the coupling of the dsDNA to the external leads can be expressed in terms of the linewidth (coupling) matrix Γ^v ($v = L, R$), that is, a $4N \times 4N$ matrix. To present the interaction between the dsDNA and two leads, we provide some details of the linewidth function Γ^v . The relevant matrix element, $\Gamma_{ij\sigma}^v = 2\pi |t_v|^2 \rho_\sigma^v$, describes the spin-related hybridization between the states of the v th lead and the boundary sites of the dsDNA chain, where ρ_σ^v is the density of states of electrons with spin σ in lead v . For the sake of simplicity, $\Gamma_{ij\sigma}^v$ is assumed to be constant within the electron bandwidth for transport.

For $v = L$ and $\sigma = \uparrow$, $\Gamma_{ij\uparrow}^L = \Gamma^L(1 + p_L)$ with $(i = j = 1)$; $\Gamma_{ij\uparrow}^L = \lambda \Gamma^L(1 + p_L)$ with $(i = j = 2)$; and $\Gamma_{ij\uparrow}^L = \gamma_L \sqrt{\Gamma_{ii\uparrow}^L \Gamma_{jj\uparrow}^L} = \gamma_L \sqrt{\lambda} \Gamma^L(1 + p_L)$ with $(i = 1, j = 2)$ or $(i = 2, j = 1)$. For $v = L$ and $\sigma = \downarrow$, $\Gamma_{ij\downarrow}^L = \Gamma^L(1 - p_L)$ with $(i = j = 2N + 1)$; $\Gamma_{ij\downarrow}^L = \lambda \Gamma^L(1 - p_L)$ with $(i = j = 2N + 2)$; and $\Gamma_{ij\downarrow}^L = \gamma_L \sqrt{\Gamma_{ii\downarrow}^L \Gamma_{jj\downarrow}^L} = \gamma_L \sqrt{\lambda} \Gamma^L(1 - p_L)$ with $(i = 2N + 1, j = 2N + 2)$ or $(i = 2N + 2, j = 2N + 1)$. In addition, for $v = R$ and $\sigma = \uparrow$, $\Gamma_{ij\uparrow}^R = \lambda \Gamma^R(1 + p_R)$ with $(i = j = 2N - 1)$; $\Gamma_{ij\uparrow}^R = \Gamma^R(1 + p_R)$ with $(i = j = 2N)$; and $\Gamma_{ij\uparrow}^R = \gamma_R \sqrt{\Gamma_{ii\uparrow}^R \Gamma_{jj\uparrow}^R} = \gamma_R \sqrt{\lambda} \Gamma^R(1 + p_R)$ with $(i = 2N - 1, j = 2N)$ or $(i = 2N, j = 2N - 1)$. For $v = R$ and $\sigma = \downarrow$, $\Gamma_{ij\downarrow}^R = \lambda \Gamma^R(1 - p_R)$ with $(i = j = 4N - 1)$; $\Gamma_{ij\downarrow}^R = \Gamma^R(1 - p_R)$ with $(i = j = 4N)$; and $\Gamma_{ij\downarrow}^R = \gamma_R \sqrt{\Gamma_{ii\downarrow}^R \Gamma_{jj\downarrow}^R} = \gamma_R \sqrt{\lambda} \Gamma^R(1 - p_R)$ with $(i = 4N - 1, j = 4N)$ or $(i = 4N, j = 4N - 1)$. $\Gamma_{ij\sigma}^v = 0$ otherwise.

Here, Γ^v and p_v are the coupling constant and the spin polarization, respectively, of the v th lead. We assume that the magnetic electrodes are similar, i.e., $\Gamma^L = \Gamma^R = 1$ eV. The parameters γ_L and γ_R are complex and different in the general case, but we assume that they are real. Since λ describes the differences in the coupling of the two edge sites to the external leads, λ can characterize the geometrical asymmetry of the system ($\lambda = 1$ implies a symmetrical configuration). In the off-diagonal matrix elements of Γ^v , γ_L (γ_R) represents the quantum interference effects due to the indirect coupling of edge sites via the leads, and $\gamma_L < 1$ ($\gamma_R < 1$) means the existence of destructive quantum interference. Indeed, the couplings between the dsDNA and the two leads can be varied in experiments; we focus mainly on symmetrical couplings ($\lambda = 1$ and $\gamma_L = \gamma_R = 1$) in the main text. The values selected for the parameters were also used in Refs. [34,35,62,63]. Additionally, the thermoelectric behavior of this system under the condition of asymmetrical couplings is presented in the Appendix.

B. Theoretical formulations of thermoelectric transport

In order to study the thermoelectric characteristics of the chiral dsDNA-based system, we use a phenomenological theoretical framework (viz., linear response theory) to describe the charge current $I = \sum_\sigma I_\sigma$ and heat (energy) current $I_Q = \sum_\sigma I_\sigma^Q$ through the dsDNA molecule device:

$$\begin{pmatrix} I \\ I_Q \end{pmatrix} = \sum_\sigma \begin{pmatrix} e^2 K_{0\sigma} & \frac{e}{T} K_{1\sigma} \\ e K_{1\sigma} & \frac{1}{T} K_{2\sigma} \end{pmatrix} \begin{pmatrix} \Delta V \\ \Delta T \end{pmatrix}, \quad (6)$$

where I_σ and I_σ^Q are the charge and heat currents, respectively, in the spin channel σ . ΔV and ΔT are the voltage drop and the temperature difference, respectively, between the two leads. The spin-dependent Onsager coefficients $K_{n\sigma}$ ($n = 0, 1, 2$) are given by

$$K_{n\sigma}(\mu, T) = -\frac{1}{h} \int d\varepsilon (\varepsilon - \mu)^n T_\sigma(\varepsilon) \frac{\partial f(\varepsilon)}{\partial \varepsilon}. \quad (7)$$

Here, $f(\varepsilon) = \{1 + \exp[(\varepsilon - \mu)/k_B T]\}^{-1}$ is the equilibrium (zero-bias) Fermi-Dirac distribution function with chemical potential μ and temperature T . $T_\sigma(\varepsilon) = \text{Tr}[\mathbf{G}_\sigma^A(\varepsilon) \mathbf{\Gamma}^R \mathbf{G}_\sigma^R(\varepsilon) \mathbf{\Gamma}^L]$ is the spin-related transmission coefficient for electrons of energy ε , where $\mathbf{G}_\sigma^{R(A)}(\varepsilon)$ is the retarded (or advanced) Green's function of the system.

The spin-dependent thermopower S_σ is defined as the ratio of the voltage drop ΔV to the temperature difference ΔT under the condition of vanishing of the spin-related

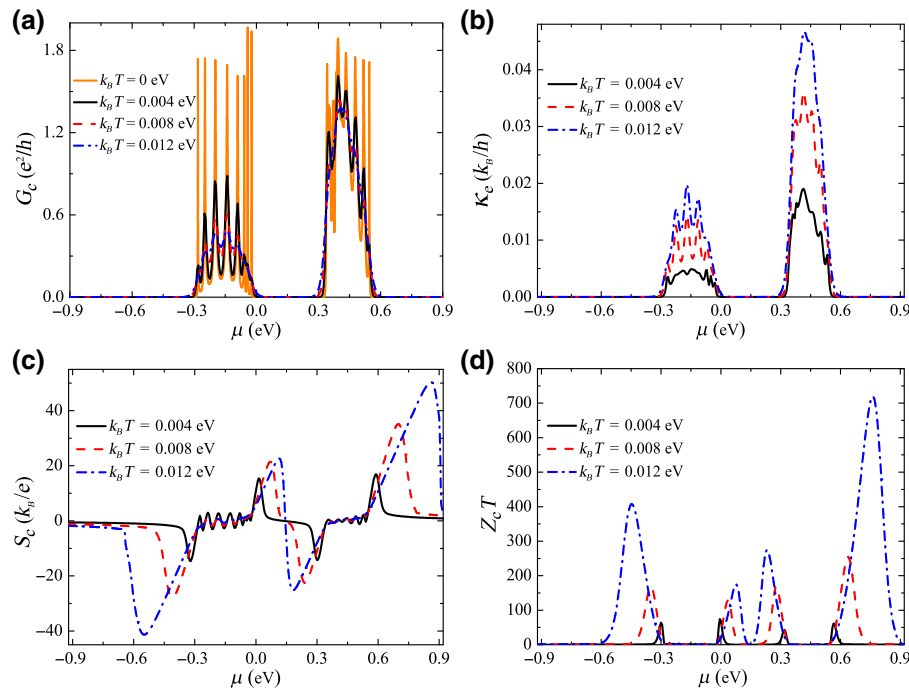


FIG. 2. (a) Linear conductance G_c , (b) thermal conductance κ_e , (c) thermopower S_c , and (d) figure of merit $Z_c T$ as functions of the chemical potential μ for different temperatures, with $p_L = p_R = p = 0.6$, $t_{so} = 0.01$ eV, and $N = 10$.

current, $I_\sigma = 0$:

$$S_\sigma(\mu, T) = \left(\frac{\Delta V}{\Delta T} \right)_{I_\sigma=0} = -\frac{1}{eT} \frac{K_{1\sigma}(\mu, T)}{K_{0\sigma}(\mu, T)}; \quad (8)$$

other spin-related quantities, including the spin-resolved conductance G_σ and spin-resolved thermal conductance $\kappa_{e\sigma}$, can be calculated as

$$\begin{aligned} G_\sigma(\mu, T) &= e^2 K_{0\sigma}(\mu, T), \quad \kappa_{e\sigma}(\mu, T) \\ &= \frac{1}{T} \left[K_{2\sigma}(\mu, T) - \frac{K_{1\sigma}^2(\mu, T)}{K_{0\sigma}(\mu, T)} \right]. \end{aligned} \quad (9)$$

Thus, the charge and spin thermoelectric coefficients of the system can be obtained from the following formulas:

$$G_c = G_\uparrow + G_\downarrow, \quad G_s = G_\uparrow - G_\downarrow, \quad (10)$$

$$S_c = S_\uparrow + S_\downarrow, \quad S_s = S_\uparrow - S_\downarrow. \quad (11)$$

Furthermore, the charge and spin thermoelectric figures of merit are given by

$$Z_c T = \frac{G_c S_c^2 T}{\kappa_e + \kappa_{ph}}, \quad Z_s T = \frac{|G_s| S_s^2 T}{\kappa_e + \kappa_{ph}}, \quad \kappa_e = \kappa_{e\uparrow} + \kappa_{e\downarrow}, \quad (12)$$

where κ_{ph} is the phonon contribution to the thermal conductance. This term, however, will not be considered in

this paper; this mainly stems from the fact that we concentrate on elastic transport process, where only electrons contribute effectively to thermal transport. In what follows, we will use the above formulas to investigate the thermoelectric properties of the chiral dsDNA thermoelectric system.

III. NUMERICAL RESULTS AND DISCUSSION

In this section we present and discuss numerical results on the thermoelectric properties of the chiral dsDNA molecule device. For the dsDNA, $\varepsilon_{1n} = 0$ eV, $\varepsilon_{2n} = 0.3$ eV, $t_{1n} = t_1 = 0.12$ eV, $t_{2n} = t_2 = -0.1$ eV, and $\lambda_n = -0.2$ eV; these values come from first-principles calculations [64,65]. The helix angle and the twist angle are taken as $\theta = 0.66$ rad and $\Delta\varphi = \pi/5$, and these two parameters are used throughout this paper, unless it is needed to indicate other values explicitly. Furthermore, we consider a parallel (P) configuration with $p_L = p_R = p$, and an antiparallel (AP) one with $p_L = -p_R = p$.

A. Charge thermoelectric effects

As is well known, the position of the chemical potential μ of the electrons is an important factor determining the thermoelectric behavior of a given system. Although μ is usually associated with the operating temperature, it exhibits a weak temperature dependence at low temperatures. Therefore, we ignore the influence of the temperature

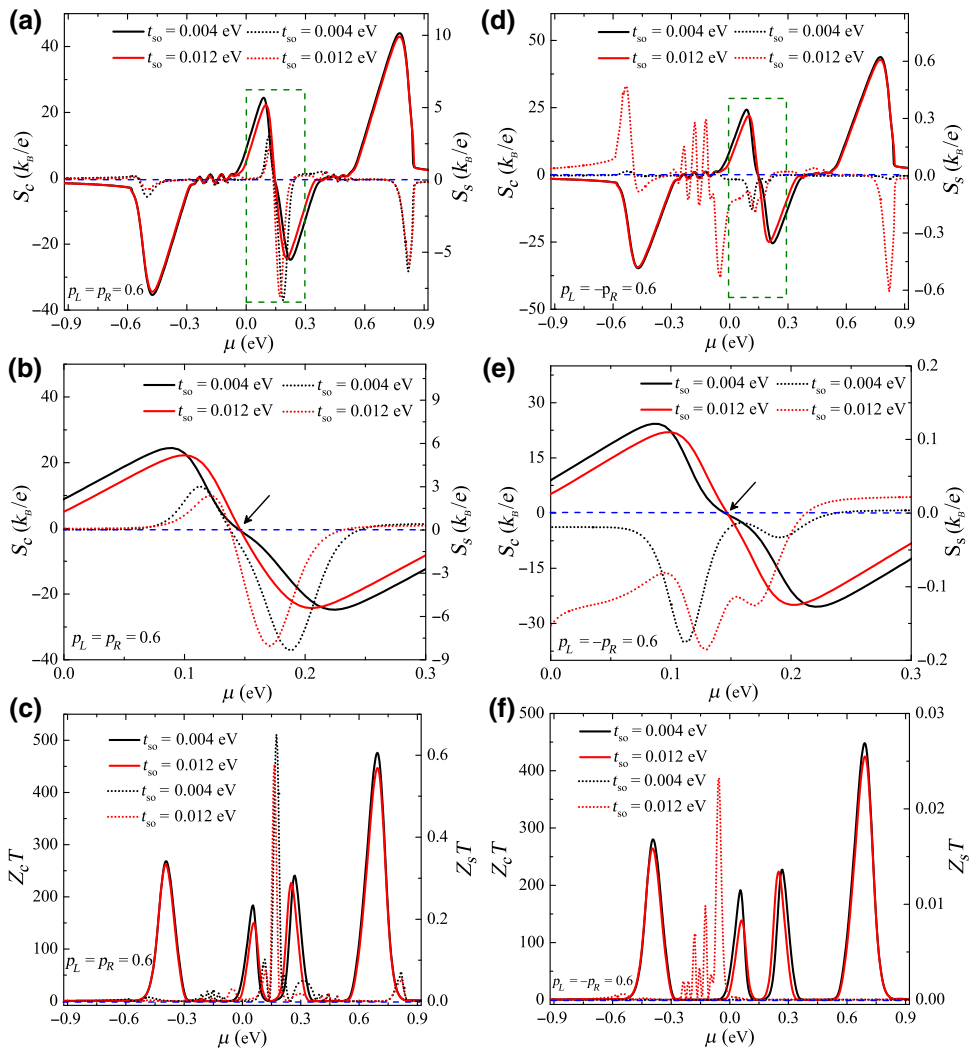


FIG. 3. Left column, S_c ($Z_c T$) (solid line) and S_s ($Z_s T$) (dotted line) as functions of the chemical potential μ for the P configuration at different spin-orbit coupling strengths t_{so} . Panel (b) is an enlarged image of the region in the dashed-line box in panel (a). The opposite cases are also shown in the right column for the AP configuration. Other parameters are taken as $k_B T = 0.01$ eV and $N = 10$.

on the chemical potential in studying thermoelectric properties. Moreover, μ can be manipulated in some ways, such as chemical doping and a gating potential, to shift the chemical potential.

To better understand the thermoelectric behavior of chiral dsDNA coupled to FM leads, we first show the dependence of the thermoelectric coefficients on the chemical potential μ for selected values of temperature, as illustrated in Fig. 2. In fact, at zero temperature, the conductance $G_c(\mu)$ is proportional to the transmission coefficient $T_c(\mu) = \sum_\sigma T_\sigma(\mu)$ based on the Landauer formula, that is, $G_c(\mu) = (e^2/h)T_c(\mu)$. As can be seen from Fig. 2(a) (see the orange solid curve), the conductance spectra at zero temperature clearly display two bands separated by a well-defined band gap (here we refer to the two bands as the highest occupied molecular orbital and the lowest unoccupied molecular orbital in the energy spectrum), and

a series of peaks occur as the chemical potential μ (i.e., Fermi energy E_F) aligns with the energy of an electron state in the dsDNA. The wave functions of the states are approximately standing-wave cases with wave vector k , and the oscillating transmission spectra can also be understood as the result of quantum tunneling when electron waves propagate from one lead to the other. As a result, the period of oscillation δE_F , which is equal to the energy difference between two neighboring energy levels in the dsDNA, is roughly determined by the relation $\delta k_F L_d \approx \pi$. Here the corresponding variation of the Fermi wave vector δk_F is equal to the wave vector difference of the two neighboring levels, and L_d is the geometric length of the dsDNA.

Furthermore, one can see that the conductance becomes suppressed as the temperature grows, since the average tunneling probability of electrons decreases with

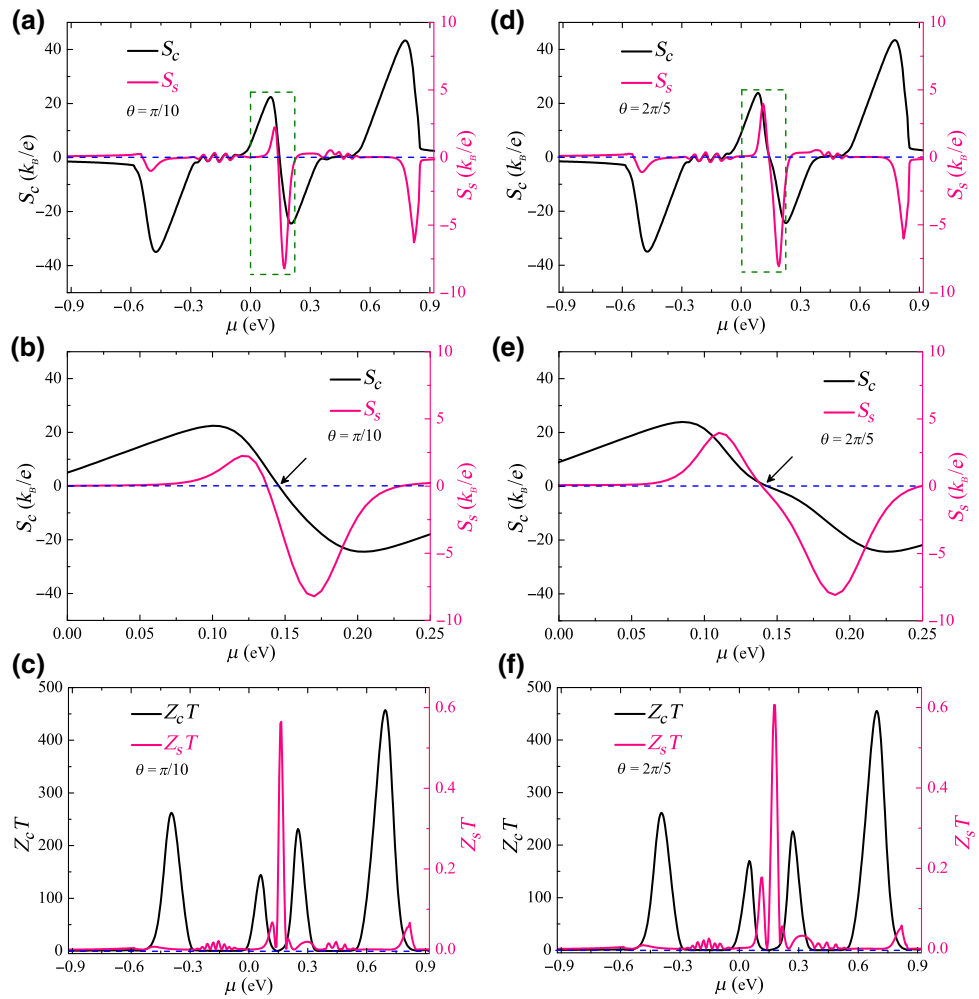


FIG. 4. Left column, S_c (S_s) and $Z_c T$ ($Z_s T$) as functions of the chemical potential μ for $\theta = \pi/10$. Panel (b) is an enlarged image of the region in the dashed-line box in panel (a). Similar cases are shown in the right column for $\theta = 2\pi/5$. Other parameters are taken as $k_B T = 0.01$ eV, $t_{so} = 0.01$ eV, $p = 0.6$, and $N = 10$.

increasing temperature. The electronic thermal conductance κ_e displays similar behavior to the conductance G_c , but κ_e [in Fig. 2(b)] is more sensitive to a change in temperature, and κ_e increases significantly with an increase in $k_B T$, which arises from the fact that an increase in temperature leads to a substantial enhancement of the heat transferred by each electron. The curves of the charge thermopower S_c as described in Fig. 2(c) are not strictly antisymmetric with respect to the electron-hole symmetry point near $\mu = 0.15$ eV, where the thermopower induced by the electrons is canceled by that of the holes and thus the total thermopower vanishes. The asymmetry of the thermopower curves is induced by the asymmetry of the dsDNA-molecule structure. Note that some other zero points ($S_c = 0$) can also be found in Fig. 2(c), and S_c changes its sign alternately when μ sweeps through these points. Thus, S_c exhibits oscillatory behavior. Indeed, two types of carriers (holes and electrons) contribute to the Seebeck transport in each energy band. For the thermopower,

$S_e < 0$ is generated by electrons, and $S_h > 0$ by holes. Thus, the sign of $S_c = S_e + S_h$ is determined by the absolute magnitudes of S_e and S_h . Consequently, $S_c < 0$ ($S_c > 0$) means that main carriers are electrons (holes). Notably, S_c is significantly enhanced near some zero points, because the transmission function changes sharply near these positions [see the zero-temperature conductance in Fig. 2(a)], and the thermopower is also enhanced as $k_B T$ grows. This can in principle contribute to a large figure of merit $Z_c T$, as shown in Fig. 2(d). It is found that a large or even giant thermoelectric efficiency can be obtained due to a strong violation of the WF law, and $Z_c T$ can be considerably enhanced as the temperature is increased, which is helpful for improving the thermoelectric efficiency in the high-temperature regime. Particularly, although both the conductance G_c and the thermal conductance κ_e are very weak within a band gap [see Figs. 2(a) and 2(b)], a considerable figure of merit $Z_c T$ can still be achieved, as depicted in Fig. 2(d). This is because the contributions from G_c and

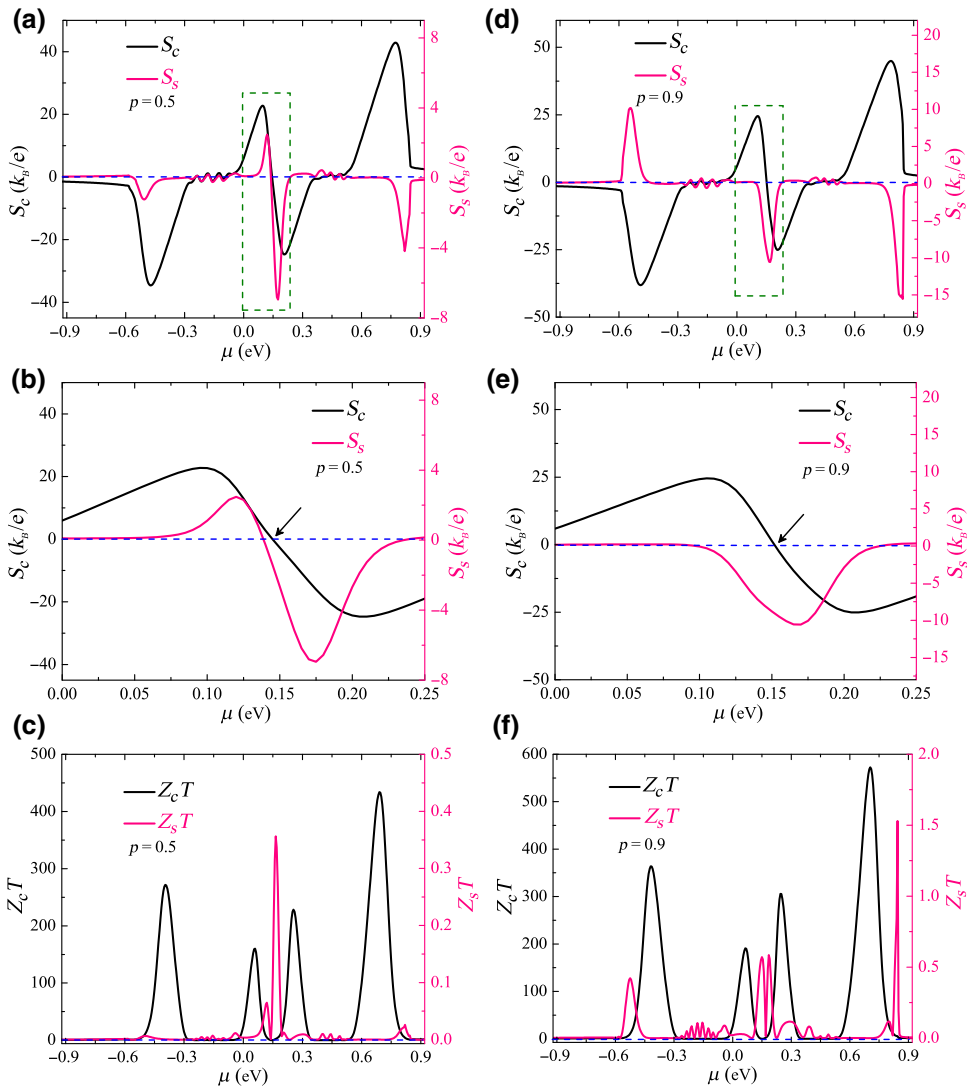


FIG. 5. Left column, S_c (S_s) and Z_cT (Z_sT) as functions of the chemical potential μ for $p = 0.5$. Panel (b) is an enlarged image of the region in the dashed-line box in panel (a). Similar cases are shown in the right column for $p = 0.9$. Other parameters are taken as $k_B T = 0.01$ eV, $t_{so} = 0.01$ eV, and $N = 10$.

κ_e to Z_cT can cancel each other [see Eq. (12)], and thus one can obtain a strong thermoelectric efficiency. Physically, in comparison with the electrical conductance, the thermal conductance is suppressed more quickly within the band gap, and then a large enhancement of S_c and Z_cT can be achieved.

B. Spin thermoelectric effects

Since the thermoelectric behavior of the chiral dsDNA system relies on the arrangement of the FM leads, we next analyze the spectra of the thermopower and the figure of merit for selected SOC values in the P and AP configurations. As we can see from Figs. 3(a) and 3(d), the charge thermopower S_c does not exhibit a pronounced response to changes in the magnetic configuration and the SOC.

As is known, the contributions from electrons and holes mostly determine the nature of S_c , and the change in S_c ($= S_{\uparrow} + S_{\downarrow}$) with μ in different magnetic configurations is weak with an increase in the SOC, but S_s ($= S_{\uparrow} - S_{\downarrow}$), displays an evident dependence on the magnetic configuration and the SOC [see Figs. 3(a), 3(b), 3(d), and 3(e)]. Moreover, the differences in G_c (and also κ_e) in the two types of configuration are also weak (not shown). Noticeably, the spin thermopower S_s is very sensitive to the magnetic configuration and the SOC [see the black and red dotted lines in Figs. 3(a) and 3(d)]. For a clearer illustration, Figs. 3(b) and 3(e) show enlarged images of the regions in the dashed-line boxes in panels (a) and (d). Interestingly, one finds that a non-zero spin-Seebeck coefficient can be produced with a vanishing S_c . Furthermore, the magnitude of the pure S_s can be enhanced by increasing the SOC [see

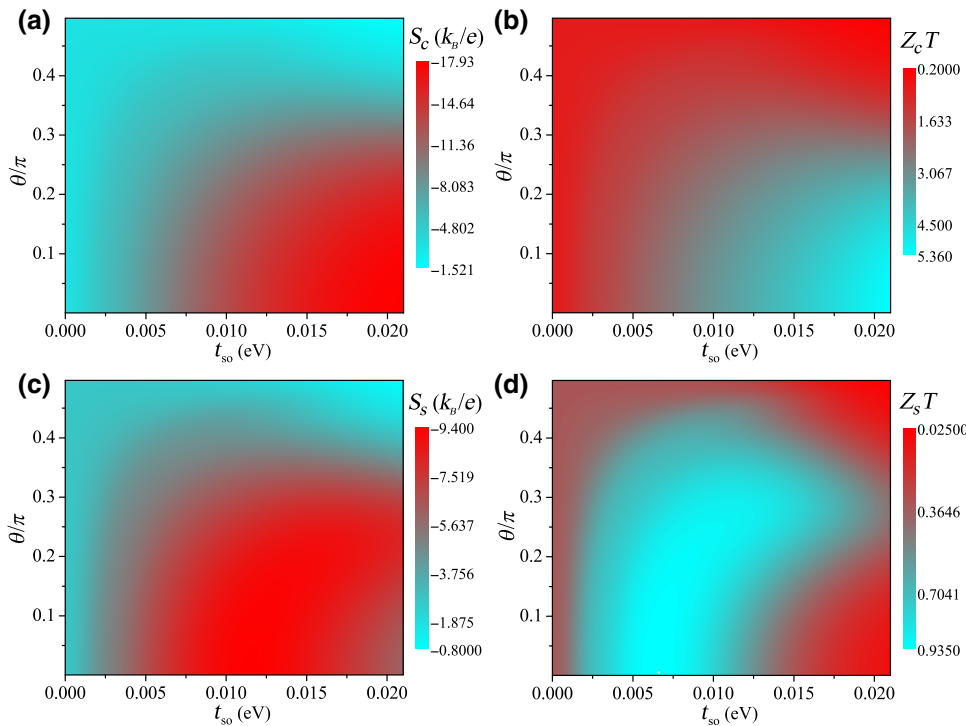


FIG. 6. S_c ($Z_c T$) and S_s ($Z_s T$) as functions of t_{so} and θ for the P configuration. Other parameters are taken as $\mu = 0.165$ eV, $k_B T = 0.01$ eV, $p = 0.7$, and $N = 10$.

the positions indicated by arrows in Figs. 3(b) and 3(e)], which means practically that a perfect spin-Seebeck effect may be used to design a pure spin-current generator. The behavior of the Seebeck coefficients (S_c and S_s) are also reflected in the curves of the figures of merit ($Z_c T$ and $Z_s T$), as illustrated in Figs. 3(c) and 3(f). It is worth noting that the spin figures of merit are usually larger for the P configuration than for the AP configuration. This can be understood from the following fact: in the P configuration, there exists one spin channel with a high conductance [corresponding to a high density of states (DOS) in the two FM leads] and one with a low conductance (corresponding to a low DOS in the two FM leads). In turn, in the AP configuration, the conductance is reduced in the two spin channels, because a high DOS in one lead corresponds to a low DOS in the other, and vice versa. Thus, $|G_s|$ (not shown) and S_s [see Fig. 3(b)] in the P configuration are larger than those in the AP configuration. Besides, the difference between the heat conductances in the two configurations is rather small. As a result, the P configuration favors an increase in S_s ($Z_s T$).

Although similar characteristics can be displayed in the AP configuration, the P arrangement, as a physically valid configuration, can better show the spin-dependent Seebeck transport; see Fig. 3. Accordingly, in what follows we focus mainly on the thermoelectricity of the P configuration. Because the helix angle θ can characterize the chirality of the dsDNA molecule, the thermoelectric

quantities S_c (S_s) and $Z_c T$ ($Z_s T$) are shown in Fig. 4 as a function of μ for different values of θ . We can observe that S_c and $Z_c T$ versus μ are weakly sensitive to the helix angle. In contrast, S_s and $Z_s T$ display an active response to a change in θ , i.e., S_s and $Z_s T$ grow with increasing θ . Nevertheless, note that the pure spin-Seebeck coefficient at $\theta = \pi/10$ is larger than that at $\theta = 2\pi/5$ [see the positions indicated by arrows in Figs. 4(b) and 4(e)]. We also note that the variation of S_s with θ is not always monotonic for different t_{so} [see Fig. 6(c)], but at $t_{\text{so}} = 0.01$ eV, an increase in θ induces a decline in the chiral helical symmetry, and thus the pure spin-Seebeck coefficient is reduced due to the weak CISS effect.

Figure 5 shows the properties of the charge (spin) thermopower S_c (S_s) as a function of μ for different polarizations p . It is seen that the dependence of S_c on p is very weak, as discussed in Refs. [31] and [34], but S_s is distinctly enhanced as p is increased. The polarization of the FM leads can influence the spin-Seebeck transport, because the FM reservoirs provide two kinds of unequal spin-up and spin-down electrons. Increasing p can induce a larger spin imbalance, and therefore the spin-Seebeck coefficients will be enhanced to some extent in some regions [see the pink lines in Figs. 5(a), 5(b), 5(d), and 5(e)]. Analogously, a finite S_s with $S_c = 0$ can also be achieved. It is well known that the charge $Z_c T$ and the spin counterpart $Z_s T$ are jointly determined by the behaviors of several physical quantities, that is, G_c (G_s), S_c (S_s), κ_e , and T .

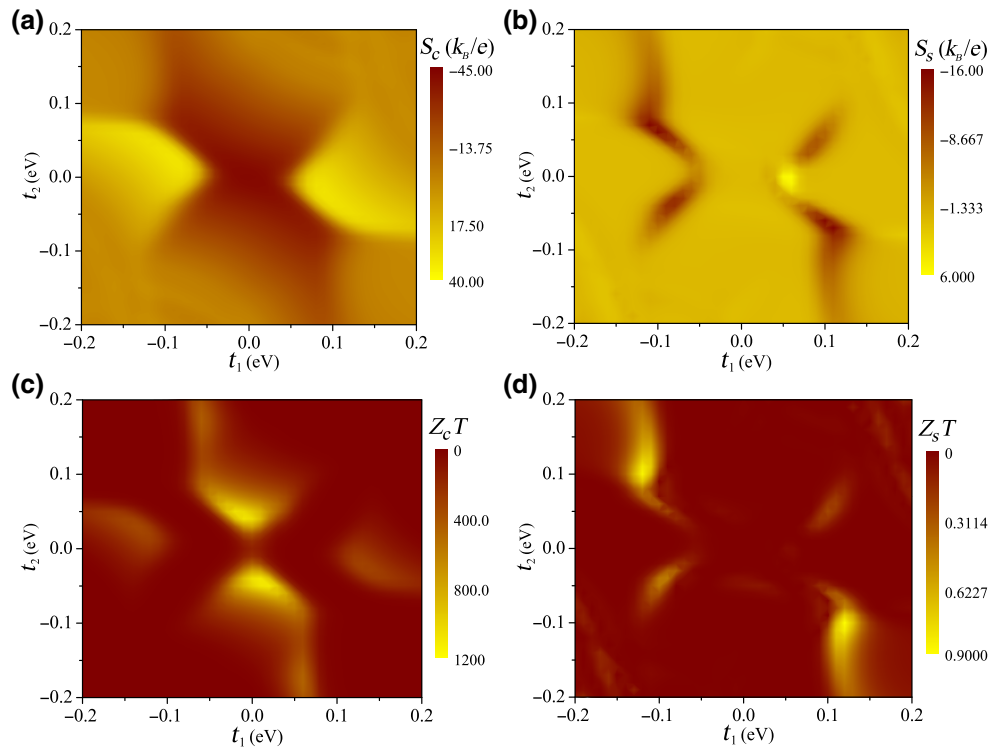


FIG. 7. S_c , S_s , $Z_c T$, and $Z_s T$ as functions of t_1 and t_2 for the P configuration. Other parameters are taken as $\mu = 0.165$ eV, $k_B T = 0.01$ eV, $p = 0.7$, $t_{so} = 0.01$ eV, and $N = 10$.

Consequently, the subtle variations of $Z_c T$ and $Z_s T$ are presented in Figs. 5(c) and 5(f). As we see, both $Z_c T$ and $Z_s T$ have maximum values that correspond to resonant structures in S_c and S_s . In particular, $Z_s T$ is sensitive to an increase in p , and $Z_s T$ can even be larger than one [see the pink line in Fig. 5(f)], indicating the potential application of the dsDNA molecule in spin caloritronic devices.

C. Dependence of thermoelectric quantities on intrinsic parameters

The chiral structural features of dsDNA molecules may be characterized by the helicity, and the spin selectivity resulting from the intrinsic SOC is unequivocally relevant to the chirality of dsDNA molecules. Accordingly, in order to better show how the SOC strength t_{so} and the helix angle θ affect the thermoelectric properties of the dsDNA system, the charge and spin thermoelectric coefficients are depicted as functions of t_{so} and θ in Fig. 6. When $t_{so} < 0.005$, the change in S_c is not drastic with tuning θ . In contrast, when $t_{so} > 0.005$ eV, the relative variation of S_c with θ is very pronounced. One can observe that the red region corresponds to a strong S_c as shown in Fig. 6(a), where t_{so} is relatively large but θ is relatively small. This can be explained as follows: A decrease in θ means that the distance ($\Delta h = l_a \sin \theta$) in the z -axis direction is reduced. Thus, the decreased scattering length

leads to an enhancement of the charge Seebeck transport. Meanwhile, the large SOC significantly enhances the spin-resolved transport. As a consequence, cooperation between the SOC and the helix angle may in principle enhance the thermopower S_c . As expected, in the corresponding parameter regime, $Z_c T$ is therefore enhanced, as shown in Fig. 6(b). The above scenarios reveal signals of how the charge-Seebeck transport is modulated by the SOC and the helix angle. In what follows, S_s shows a weak or monotonic variation with θ at $t_{so} < 0.0153$ eV, but at $t_{so} > 0.0153$ eV, the variation of S_s with θ shows a nonmonotonic behavior, as shown in Fig. 6(c). Similar trends can be found in $Z_s T$, as shown in Fig. 6(d). The contours of S_s and $Z_s T$ can thus reflect legible information about spin-Seebeck transport influenced by t_{so} and θ .

Since the intrastrand hopping integrals t_1 and t_2 are experimentally tuned via stretching, the detailed dependence of the thermoelectric characteristics on t_1 and t_2 is presented in Fig. 7. One can see that the thermoelectric coefficients exhibit strong geometrical contours, which nicely mirrors the various thermoelectric responses to external mechanical operations. Moreover, the sign of the charge Seebeck coefficient can be used to characterize the type of our dsDNA device, as shown in Fig. 7(a): $S_c > 0$ indicates a p -type device, while $S_c < 0$ suggests an n -type one, which means that the type of a dsDNA-based thermoelectric device may be manipulated by means

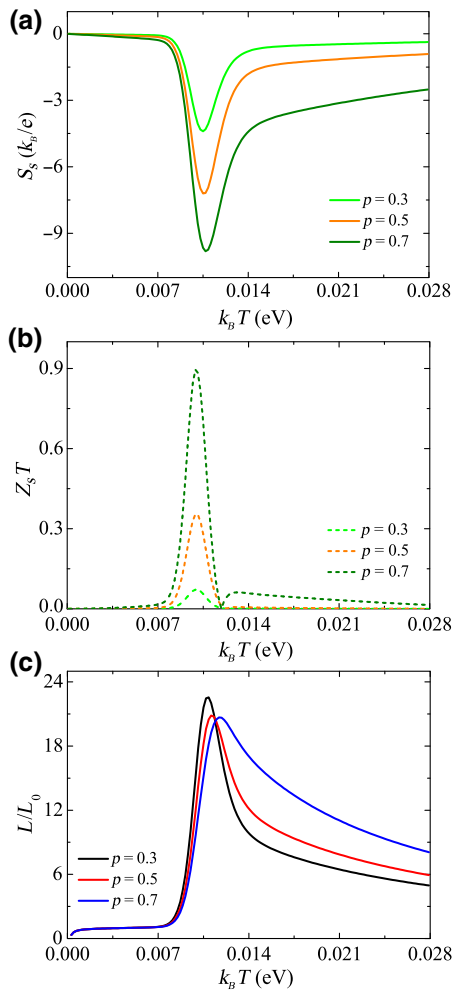


FIG. 8. (a),(b) S_s and $Z_s T$ as a function of temperature $k_B T$ for the indicated values of spin polarization p . (c) Lorentz ratio (L/L_0) as a function of temperature $k_B T$ for the indicated values of spin polarization p . Other parameters are taken as $\mu = 0.165$ eV, $t_{\text{so}} = 0.01$ eV, and $N = 10$.

of the hopping integrals. We note that the signs of the two Seebeck coefficients (S_c and S_s) can be changed from positive to negative, which implies that it is possible to obtain a pure spin-Seebeck coefficient (i.e., S_s retains a finite value with $S_c = 0$) in some special regimes of (t_1, t_2) space. In addition, $Z_c T$ can reach a sizeable value, as illustrated in Fig. 7(c), which is a direct consequence of the hopping integrals enhancing the thermoelectric efficiency. Our results offer a practical route towards harnessing external ways to tailor the thermoelectric performance of a dsDNA-based device.

D. Influence of temperature

In Figs. 8(a) and 8(b), we illustrate the temperature dependence of S_s and $Z_s T$. One can see that the two thermoelectric quantities display nonmonotonic behavior with increasing temperature, and there exist valleys and

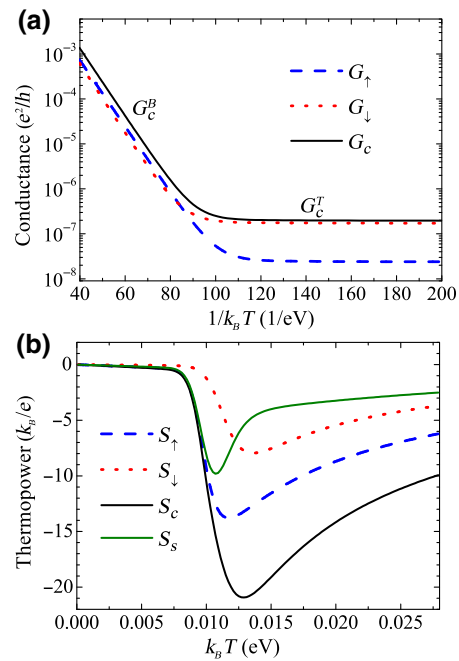


FIG. 9. (a) Spin-dependent conductances G_σ and charge conductance G_c as a function of the inverse of the temperature $k_B T$. (b) Spin-dependent thermopowers S_σ and charge (spin) thermopowers S_c (S_s) as a function of temperature $k_B T$. Other parameters are taken as $\mu = 0.165$ eV, $t_{\text{so}} = 0.01$ eV, $p = 0.7$, and $N = 10$.

peaks in the curves of S_s and $Z_s T$, respectively, around $k_B T = 0.01$ eV. With increasing polarization p , the amplitudes of the corresponding valleys and peaks are also enhanced, which means that the strong spin imbalance of carriers due to the large spin polarization of the leads can stimulate a spin-Seebeck transport process, as discussed above in relation to Fig. 5. Since nanoscale systems usually cause a violation of the WF law, we show the Lorentz ratio L/L_0 [in units of $(e/k_B)^2$] as a function of temperature $k_B T$ for selected values of p in Fig. 8(c), where $L = \kappa_e/G_c T$ and $L_0 = \pi^2 k_B^2/3e^2$. Analogously to S_s and $Z_s T$, L/L_0 as a function of $k_B T$ displays a nonmonotonic lineshape, and strongly exceeds 1, indicating a breakdown of the WF law.

We notice that an abrupt variation of the spin thermopower $|S_\sigma|$ occurs near $k_B T = 0.01$ eV, as depicted in Fig. 8(a). The underlying reasons can be understood as follows. From a mathematical point of view, according to the well-known Mott formula for the thermopower

$$S_\sigma = -\frac{\pi^2 k_B^2}{3e^2} T \frac{\partial \ln T_\sigma(\varepsilon)}{\partial \varepsilon} \Big|_\mu, \quad (13)$$

S_σ grows linearly versus $k_B T$ at low temperatures. Increasing the temperature can drive more carriers to participate in the thermoelectric transport. Simultaneously, the Fermi-Dirac distribution around the chemical potential becomes smeared with a further increase in temperature, and thus

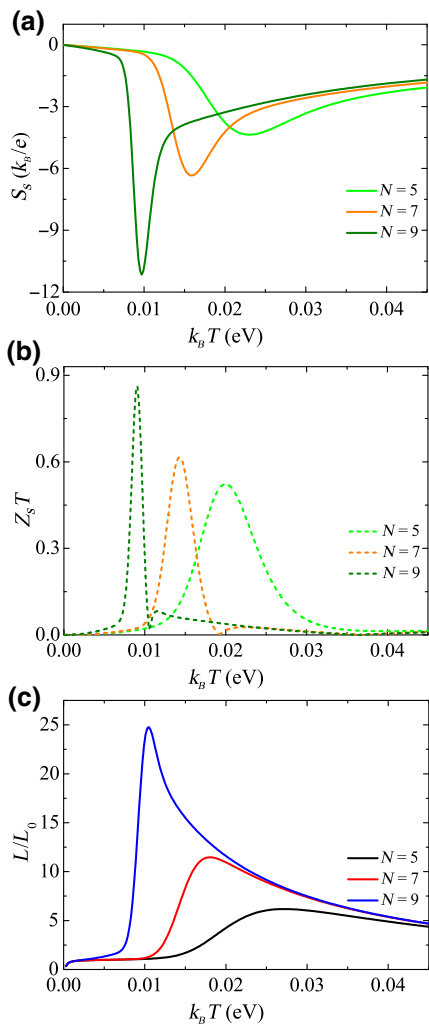


FIG. 10. (a),(b) S_s and $Z_s T$ as a function of temperature $k_B T$ for different N . (c) Lorentz ratio L/L_0 as a function of temperature $k_B T$ for different N . Other parameters are taken as $\mu = 0.165$ eV, $t_{so} = 0.01$ eV, and $p = 0.7$.

leads to the reduction of the magnitude of $-\partial f(\varepsilon)/\partial \varepsilon$, which weakens S_σ . Thereby, the interplay of the above two factors leads to an optimal temperature in the curves of $S_s = S_\uparrow - S_\downarrow$. Furthermore, the features of S_s can also be reflected in the curves of $Z_s T$ and L/L_0 according to $Z_s T \propto S_s^2$ and $L = \kappa_e/G_c T = S_c^2/Z_c T$, as shown in Figs. 8(b) and 8(c).

In order to further reveal the fundamental physics around the characteristic temperature $k_B T = 0.01$ eV, we first depict the conductances (G_σ and G_c) as a function of $1/k_B T$ in Fig. 9(a). Note that if the spin degree of freedom is not considered (under the conditions of $\theta = \pi/2$, $t_{so} = 0$, and $p = 0$), a characteristic temperature still exists (not shown here). Therefore, a simplified effective model is utilized to capture the main physical elements of the characteristic temperature. At low temperatures, the tunneling

conductance reads approximately

$$G_c^T \approx G_0 \left(\frac{t_0}{\varepsilon_0 - \mu} \right)^{2N} \frac{\Delta_L \Delta_R}{t_0^2}, \quad (14)$$

where the quantum of conductance is $G_0 = e^2/h$, the chemical potential is $\mu = 0.165$ eV, the mid energy of the nearest band is $\varepsilon_0 = 0.45$ eV, one fourth of the width of the nearest band is $t_0 = 0.075$ eV as illustrated in Fig. 2(a), and the DNA-lead couplings are $\Delta_L = \Delta_R \in [0.3, 1]$ eV. At high temperatures, the ballistic conductance is determined by the number of carriers in the bands and can be expressed as

$$G_c^B \approx G_0 \mathbb{N}_0 \exp \left\{ \frac{-|\varepsilon_0 - \mu|}{k_B T} \right\}, \quad (15)$$

where the number of states in the nearest energy band is $\mathbb{N}_0 \approx N$. At the transition temperature T^{BT} , where $G_c^T \approx G_c^B$, we get

$$k_B T^{BT} \approx \frac{|\varepsilon_0 - \mu|}{2N \ln(|\varepsilon_0 - \mu|/t_0)} \approx 0.01 \text{ eV}, \quad (16)$$

which is appropriately displayed in Fig. 9(a). Thus, the characteristic temperature originates from a transition from tunneling to ballistic transport in the dsDNA when the chemical potential is located near the middle of the energy gap [55]. One can also see that the characteristic temperature depends mainly on the length of the DNA, the width of the nearest energy band, and the distance between the chemical potential and the nearest energy band of the DNA. By means of Eqs. (8) and (11), the thermopower is obtained correspondingly, as shown in Fig. 9(b). At low temperatures, the thermopower is governed by Eq. (13), which results in a linear dependence of the thermopower on the temperature. As $k_B T$ approaches the transition temperature, ballistic transport becomes dominant and the thermopower jumps from the low-temperature linear behavior to the high-temperature inverse behavior, and thus the thermopower exhibits an abrupt variation. The high-temperature inverse behavior (viz., $S_\sigma \propto 1/k_B T$) is caused by the thermal broadening in the ballistic regime [32–34,48,55].

Finally, how the length N of the dsDNA molecule affects the thermoelectricity in terms of S_s , $Z_s T$, and L/L_0 is presented in Fig. 10. One can observe dips and peaks that are analogous to those in Fig. 8. The detailed descriptions of the above-mentioned physical mechanisms also pertain to this case. As illustrated in Fig. 10, the positions of the dips and peaks are shifted towards higher temperatures with decreasing N . Similar observations are also presented in Ref. [46]. Note that stronger spin-Seebeck transport can be realized at higher temperatures for shorter dsDNA chains, as shown in Figs. 10(a) and 10(b). Meanwhile, a strong

violation of the WF law also emerges at high temperatures [Fig. 10(c)]. This may provide a possibility of improving the conversion of heat to electricity by tuning the operating temperature and the length of the dsDNA.

IV. CONCLUSIONS

The CISS effect originating from the intrinsic features of chiral molecules unequivocally induces spin-dependent thermoelectric transport when a chiral molecule coupled to external leads is driven by a temperature difference. In this paper, we explore the thermoelectric properties of a chiral dsDNA molecule attached to two FM leads. The underlying physics of the oscillating peaks in the conductance as a function of the chemical potential is elaborated on. In some special regimes, both the thermopower and the figure of merit have large values, and even a giant thermoelectric efficiency can be obtained, which implies a strong violation of the WF law. When the configuration of the magnetic leads is varied from parallel to antiparallel, similar characteristics also occur but are inconspicuous compared with the parallel configuration. Specifically, we concentrate on the spin analogs of the thermopower and figure of merit (the so-called spin-Seebeck coefficient and spin figure of merit), and find that the two spin thermoelectric quantities are evidently related to the SOC, the helix angle, and the spin polarization of the leads. Interestingly, a finite spin-Seebeck coefficient with a vanishing

charge-Seebeck coefficient can be obtained; moreover, the pure spin-Seebeck coefficient has an explicit dependence on the chiral nature of the dsDNA. From the application point of view, this may be utilized to construct a spin-current generator. Besides, the spin figure of merit may be larger than unity, which is linked to the strong asymmetry of the two spin channels.

We also investigate the behavior of the charge and spin thermoelectric quantities as functions of the SOC and the helix angle, and find that cooperation between the SOC and the helix angle may enhance the thermoelectric transport. The explicit dependence of the thermopower and figure of merit on the intrastrand hopping integrals for the dsDNA demonstrates that the intrinsic nature of dsDNA molecules can provide a promising ingredient for tuning the thermoelectric performance via experimental means. Furthermore, a stronger spin polarization of the leads and longer dsDNA favor the enhancement of the spin thermoelectric quantities, and the WF law can be overcome. Meanwhile, the physics behind the characteristic temperature, where an abrupt variation of several thermoelectric quantities occurs, is presented.

As far as the practical realization of this chiral-dsDNA thermoelectric model is concerned, it may be possible to fabricate such a dsDNA molecular junction via current advanced techniques in nanoscience and organic molecular electronic materials. Our results may contribute to an in-depth understanding of spin-related Seebeck

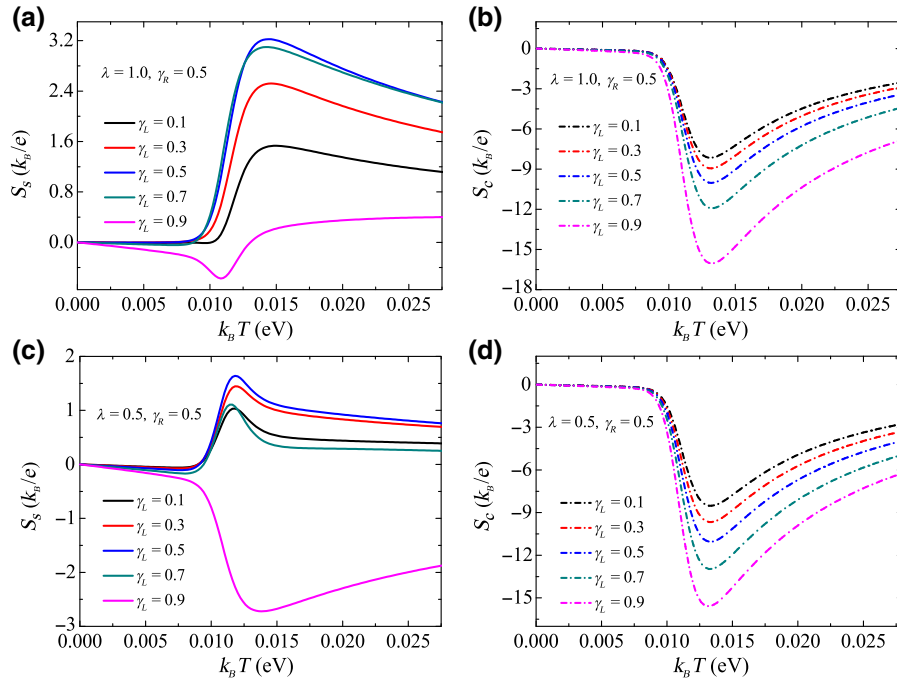


FIG. 11. (a),(b) S_s and S_c as a function of temperature $k_B T$ for different γ_L at fixed $\lambda = 1.0$ and $\gamma_R = 0.5$. (c),(d) S_s and S_c as a function of temperature $k_B T$ for different γ_L at fixed $\lambda = 0.5$ and $\gamma_R = 0.5$. Other parameters are taken as $\mu = 0.165$ eV, $t_{so} = 0.01$ eV, $p = 0.7$, and $N = 10$.

transport through chiral molecules, and be beneficial for the application of thermoelectricity based on chiral molecules.

ACKNOWLEDGMENTS

This work is financially supported by the National Natural Science Foundation of China (Grant Nos. 11104346, 61674110, and 11874016). R.-Q.W. acknowledges support from the Key Program for Guangdong NSF of China (Grant No. 2017B030311003). We would like to thank B. Dong, Tao Hou, Y. S. Liu, Lin Li, Jun Zheng, Yong Guo, and H. Z. Tang for helpful discussions. As well, we thank the anonymous referees for their constructive comments.

APPENDIX THERMOELECTRIC FEATURES IN THE PRESENCE OF ASYMMETRICAL COUPLINGS

The Seebeck coefficient is of high significance, specifically in the context of thermoelectricity. Therefore, we present mainly the Seebeck coefficients of the dsDNA magnetic junction under the condition of asymmetrical couplings here. Under the condition of structural symmetry ($\lambda = 1.0$) and imperfect interference ($\gamma_R = 0.5$), S_s and S_c are illustrated in Figs. 11(a) and 11(b) as functions of $k_B T$ for the indicated values of γ_L . One observes that S_s and S_c exhibit nonmonotonic behavior. The physics behind the peaks or valleys in the curves of the thermopowers can be qualitatively understood from the explanations for Figs. 8

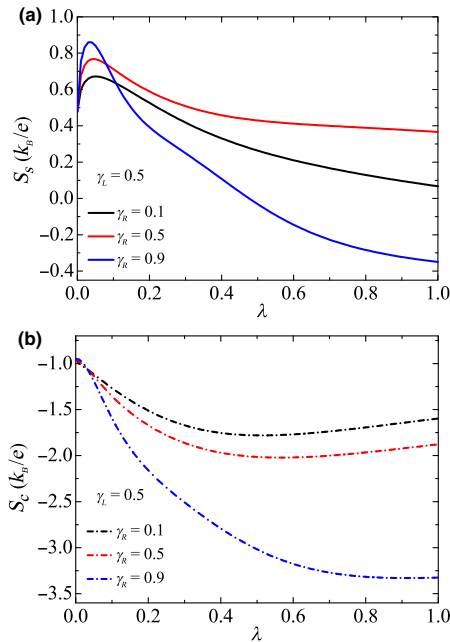


FIG. 12. (a) At fixed $\gamma_L = 0.5$, S_s as a function of λ for different γ_R . (b) At fixed $\gamma_L = 0.5$, S_c as a function of λ for different γ_R . Other parameters are taken as $\mu = 0.165$ eV, $t_{\text{so}} = 0.01$ eV, $p = 0.7$, $k_B T = 0.01$ eV, and $N = 10$.

and 9. Note that the matching ratio $\gamma = \gamma_L/\gamma_R$ between the indirect coupling factors γ_L and γ_R can be used to adjust S_s and S_c . As can be seen from Fig. 11(a), S_s first increases with γ for $\gamma \leq 1$ and then decreases with further increase in γ for $\gamma > 1$. Remarkably, the sign of S_s can be altered by adjusting γ . We can observe that the magnitudes of $|S_c|$ are enhanced with an increase in γ , as shown in Fig. 11(b). For a geometrical asymmetry ($\lambda = 0.5$) and imperfect interference ($\gamma_R = 0.5$), similar properties are explicitly shown in Figs. 11(c) and 11(d). The subtle differences between S_s and S_c for the indicated values of λ originate from the geometrical difference of this system.

In order to further reveal how the geometrical parameter λ influences the features of the thermopower under the condition of imperfect quantum interference, S_s and S_c are presented as functions of λ for selected values of γ_L and γ_R in Figs. 12(a) and 12(b), respectively. For small values of λ (strong asymmetry), S_s increases with increasing matching ratio $\gamma' = \gamma_R/\gamma_L$, while for large values of λ (strong symmetry), S_s decreases with increasing matching ratio γ' . It is interesting to note that the sign of S_s can be adjusted by tuning γ' . In contrast to S_s , we find that the asymptotic geometrical symmetry of this system (i.e., λ is close to 1) is advantageous for enhancing S_c with a strong γ' .

- [1] D. D. Eley and D. I. Spivey, Semiconductivity of organic substances, *Trans. Faraday Soc.* **58**, 411 (1962).
- [2] K. H. Yoo, D. H. Ha, J. O. Lee, J. W. Park, J. Kim, J. J. Kim, H. Y. Lee, T. Kawai, and H. Y. Choi, Electrical Conduction through Poly(dA)-Poly(dT) and Poly(dG)-Poly(dC) DNA Molecules, *Phys. Rev. Lett.* **87**, 198102 (2001).
- [3] A. J. Storm, J. van Noort, S. de Vries, and C. Dekker, Insulating behavior for DNA molecules between nanoelectrodes at the 100 nm length scale, *Appl. Phys. Lett.* **79**, 3881 (2001).
- [4] H. W. Fink and C. Schönenberger, Electrical conduction through DNA molecules, *Nature (London)* **398**, 407 (1999).
- [5] B. Hartzell, B. McCord, D. Asare, H. Chen, J. J. Heremans, and V. Soghomonian, Comparative current-voltage characteristics of nicked and repaired λ -DNA, *Appl. Phys. Lett.* **82**, 4800 (2003).
- [6] A. Y. Kasumov, D. V. Klinov, P. E. Roche, S. Gueron, and H. Bouchiat, Thickness and low-temperature conductivity of DNA molecules, *Appl. Phys. Lett.* **84**, 1007 (2004).
- [7] M. Xu, R. G. Endres, and Y. Arakawa, The electronic properties of DNA bases, *Small* **3**, 1539 (2007).
- [8] A. Y. Kasumov, M. Kociak, S. Guéron, B. Reulet, V. T. Volkov, D. V. Klinov, and H. Bouchiat, Proximity-induced superconductivity in DNA, *Science* **291**, 280 (2001).
- [9] S. Roche, Sequence Dependent DNA-mediated Conduction, *Phys. Rev. Lett.* **91**, 108101 (2003).
- [10] X. F. Wang and T. Chakraborty, Charge Transfer via a Two-strand Superexchange Bridge in DNA, *Phys. Rev. Lett.* **97**, 106602 (2006).

- [11] G. Cuniberti, L. Craco, D. Porath, and C. Dekker, Backbone-induced semiconducting behavior in short DNA wires, *Phys. Rev. B* **65**, 241314(R) (2002).
- [12] R. Gutiérrez, S. Mandal, and G. Cuniberti, Quantum transport through a DNA wire in a dissipative environment, *Nano Lett.* **5**, 1093 (2005).
- [13] W. Ren, J. Wang, Z. Ma, and H. Guo, Dynamical conductance of model DNA sequences, *J. Chem. Phys.* **125**, 164704 (2006).
- [14] S. S. Alexandre, E. Artacho, J. M. Soler, and H. Chacham, Small Polarons in dry DNA, *Phys. Rev. Lett.* **91**, 108105 (2003).
- [15] A. Rakitin, P. Aich, C. Papadopoulos, Y. Kobzar, A. S. Vedeneev, J. S. Lee, and J. M. Xu, Metallic Conduction through Engineered DNA: DNA Nanoelectronic Building Blocks, *Phys. Rev. Lett.* **86**, 3670 (2001).
- [16] A. V. Malyshev, DNA Double Helices for Single Molecule Electronics, *Phys. Rev. Lett.* **98**, 096801 (2007).
- [17] J. Bath and A. J. Turberfield, DNA nanomachines, *Nat. Nanotechnol.* **2**, 275 (2007).
- [18] N. Kang, A. Erbe, and E. Scheer, Observation of negative differential resistance in DNA molecular junctions, *Appl. Phys. Lett.* **96**, 023701 (2010).
- [19] E. L. Albuquerque, U. L. Fulco, V. N. Freire, E. W. S. Caetano, M. L. Lyra, and F. A. B. F. de Mourad, DNA-based nanobiostrukture devices: The role of quasiperiodicity and correlation effects, *Phys. Rep.* **535**, 139 (2014).
- [20] C. Guo, K. Wang, E. Zerah-Harush, J. Hamill, B. Wang, Y. Dubi, and B. Xu, Molecular rectifier composed of DNA with high rectification ratio enabled by intercalation, *Nat. Chem.* **8**, 484 (2016).
- [21] L. Xiang, J. L. Palma, Y. Li, V. Mujica, M. A. Ratner, and N. Tao, Gate-controlled conductance switching in DNA, *Nat. Commun.* **8**, 14471 (2017).
- [22] M. Zwolak and M. Di Ventra, DNA spintronics, *Appl. Phys. Lett.* **81**, 925 (2002).
- [23] X. F. Wang and T. Chakraborty, Spin injection into a short DNA chain, *Phys. Rev. B* **74**, 193103 (2006).
- [24] B. Góler, V. Hamelbeck, T. Z. Markus, M. Kettner, G. F. Hanne, Z. Vager, R. Naaman, and H. Zacharias, Spin selectivity in electron transmission through self-assembled monolayers of double-stranded DNA, *Science* **331**, 894 (2011).
- [25] A. M. Guo and Q. F. Sun, Spin-selective Transport of Electrons in DNA Double Helix, *Phys. Rev. Lett.* **108**, 218102 (2012).
- [26] A. M. Guo and Q. F. Sun, Enhanced spin-polarized transport through DNA double helix by gate voltage, *Phys. Rev. B* **86**, 035424 (2012).
- [27] A. M. Guo and Q. F. Sun, Sequence-dependent spin-selective tunneling along double-stranded DNA, *Phys. Rev. B* **86**, 115441 (2012).
- [28] D. Rai and M. Galperin, Electrically driven spin currents in DNA, *J. Phys. Chem. C* **117**, 13730 (2013).
- [29] S. Behnia, S. Fathizadeh, and A. Akhshani, DNA spintronics: Charge and spin dynamics in DNA wires, *J. Phys. Chem. C* **120**, 2973 (2016).
- [30] Y. Dubi, and M. Di Ventra, Thermospin effects in a quantum dot connected to ferromagnetic leads, *Phys. Rev. B* **79**, 081302(R) (2009).
- [31] R. Śirkowicz, M. Wierzbicki, and J. Barnás, Thermoelectric effects in transport through quantum dots attached to ferromagnetic leads with noncollinear magnetic moments, *Phys. Rev. B* **80**, 195409 (2009).
- [32] D. M. T. Kuo and Y. Chang, Thermoelectric and thermal rectification properties of quantum dot junctions, *Phys. Rev. B* **81**, 205321 (2010).
- [33] M. Wierzbicki and R. Śirkowicz, Influence of interference effects on thermoelectric properties of double quantum dots, *Phys. Rev. B* **84**, 075410 (2011).
- [34] P. Trocha and J. Barnás, Large enhancement of thermoelectric effects in a double quantum dot system due to interference and Coulomb correlation phenomena, *Phys. Rev. B* **85**, 085408 (2012).
- [35] L. Karwacki and P. Trocha, Spin-dependent thermoelectric effects in a strongly correlated double quantum dot, *Phys. Rev. B* **94**, 085418 (2016).
- [36] J. A. Andrade and P. S. Cornaglia, Spin filtering and thermopower in star-coupled quantum dot devices, *Phys. Rev. B* **94**, 235112 (2016).
- [37] J. E. Cornett and O. Rabin, Universal scaling relations for the thermoelectric power factor of semiconducting nanostructures, *Phys. Rev. B* **84**, 205410 (2011).
- [38] V. Balachandran, R. Bosisio, and G. Benenti, Validity of the Wiedemann-Franz law in small molecular wires, *Phys. Rev. B* **86**, 035433 (2012).
- [39] Y. Qi, Z. Wang, M. Zhang, F. Yang, and X. Wang, Thermoelectric devices based on one-dimensional nanostructures, *J. Mater. Chem. A* **1**, 6110 (2013).
- [40] I. J. Chen, A. Burke, A. Svilans, H. Linke, and C. Thelander, Thermoelectric Power Factor Limit of a 1D Nanowire, *Phys. Rev. Lett.* **120**, 177703 (2018).
- [41] Y. M. Zuev, W. Chang, and P. Kim, Thermoelectric and Magnetothermoelectric Transport Measurements of Graphene, *Phys. Rev. Lett.* **102**, 096807 (2009).
- [42] C. R. Wang, W. S. Lu, L. Hao, W. L. Lee, T. K. Lee, F. Lin, I. C. Cheng, and J. Z. Chen, Enhanced Thermoelectric Power in Dual-gated Bilayer Graphene, *Phys. Rev. Lett.* **107**, 186602 (2011).
- [43] M. Saiz-Bretín, A. V. Malyshev, P. A. Orellana, and F. Domínguez-Adame, Enhancing thermoelectric properties of graphene quantum rings, *Phys. Rev. B* **91**, 085431 (2015).
- [44] Y. Xu, R. L. Chu, and C. Zhang, Enhanced Thermoelectric Performance and Anomalous Seebeck Effects in Topological Insulators, *Phys. Rev. Lett.* **112**, 136402 (2014).
- [45] N. Xu, Y. Xu, and J. Zhu, Topological insulators for thermoelectrics, *npj Quantum Mater.* **2**, 51 (2017).
- [46] D. Segal, Thermoelectric effect in molecular junctions: A tool for revealing transport mechanisms, *Phys. Rev. B* **72**, 165426 (2005).
- [47] P. Reddy, S. Y. Jang, R. A. Segelman, and A. Majumdar, Thermoelectricity in molecular junctions, *Science* **315**, 1568-1571 (2007).
- [48] D. Nozaki, H. Sevinçli, W. Li, R. Gutiérrez, and G. Cuniberti, Engineering the figure of merit and thermopower in single-molecule devices connected to semiconducting electrodes, *Phys. Rev. B* **81**, 235406 (2010).

- [49] Y. Dubi and M. Di Ventra, Heat flow and thermoelectricity in atomic and molecular junctions, *Rev. Mod. Phys.* **83**, 131 (2011).
- [50] E. Maciá, Thermoelectric power and electrical conductance of DNA based molecular junctions, *Nanotechnology* **16**, S254 (2005).
- [51] E. Maciá, DNA-based thermoelectric devices: A theoretical prospective, *Phys. Rev. B* **75**, 035130 (2007).
- [52] E. Maciá, Codon thermoelectric signature in molecular junctions, *Phys. Rev. B* **82**, 045431 (2010).
- [53] Y. J. Dong, X. F. Wang, Y. S. Liu, and X. M. Wu, Length enhancement of thermoelectric effects in DNA duplex chains due to quantum interferences, *Org. Electron.* **26**, 176 (2015).
- [54] Y. Li, L. Xiang, J. L. Palma, Y. Asai, and N. Tao, Thermoelectric effect and its dependence on molecular length and sequence in single DNA molecules, *Nat. Commun.* **7**, 11294 (2016).
- [55] R. Korol, M. Kilgour, and D. Segal, Thermopower of molecular junctions: Tunneling to hopping crossover in DNA, *J. Chem. Phys.* **145**, 224702 (2016).
- [56] S. Yeganeh, M. A. Ratner, E. Medina, and V. Mujica, Chiral electron transport: Scattering through helical potentials, *J. Chem. Phys.* **131**, 014707 (2009).
- [57] R. Naaman and D. H. Waldeck, Chiral-induced spin selectivity effect, *J. Phys. Chem. Lett.* **3**, 2178 (2012).
- [58] R. Naaman and D. H. Waldeck, Spintronics and chirality: Spin selectivity in electron transport through chiral molecules, *Annu. Rev. Phys. Chem.* **66**, 263 (2015).
- [59] S. Matityahu, Y. Utsumi, A. Aharonov, O. Entin-Wohlman, and C. A. Balseiro, Spin-dependent transport through a chiral molecule in the presence of spin-orbit interaction and nonunitary effects, *Phys. Rev. B* **93**, 075407 (2016).
- [60] S. Varela, V. Mujica, and E. Medina, Effective spin-orbit couplings in an analytical tight-binding model of DNA: Spin filtering and chiral spin transport, *Phys. Rev. B* **93**, 155436 (2016).
- [61] J. M. Abendroth, N. Nakatsuka, M. Ye, D. Kim, E. E. Fullerton, A. M. Andrews, and P. S. Weiss, Analyzing spin selectivity in DNA-mediated charge transfer via fluorescence microscopy, *ACS Nano* **11**, 7516 (2017).
- [62] P. Trocha and J. Barnás, Quantum interference and Coulomb correlation effects in spin-polarized transport through two coupled quantum dots, *Phys. Rev. B* **76**, 165432 (2007).
- [63] P. Trocha, The role of the indirect tunneling processes and asymmetry in couplings in orbital Kondo transport through double quantum dots, *J. Phys.: Condens. Matter* **24**, 055303 (2012).
- [64] R. G. Endres, D. L. Cox, and R. R. P. Singh, Colloquium: The quest for high-conductance DNA, *Rev. Mod. Phys.* **76**, 195 (2004).
- [65] K. Senthilkumar, F. C. Grozema, C. F. Guerra, F. M. Bickelhaupt, F. D. Lewis, Y. A. Berlin, M. A. Ratner, and L. D. A. Siebbeles, Absolute rates of hole transfer in DNA, *J. Am. Chem. Soc.* **127**, 14894 (2005).